JOURNAL OF SOLID STATE CHEMISTRY **124,** 272–277 (1996)
ARTICLE NO. 0236

Crystal Structure of $TbTa_3O_9$ and $EuTa_3O_9$ and Their Continuous Solid Solution Characterization

A. Ibarra-Palos and M. E. Villafuerte-Castrejón

Instituto de Investigaciones en Materiales, Universidad Nacional Autónoma de México, A.P. 70-360, Ciudad Universitaria, Coyoacán 04510, México, D.F.

J. Duque

Centro Nacional de Investigaciones Científicas, P.O. Box E990, Havana, Cuba

and

R. Pomés

CINVESTAV (IPN), Mérida, A.P. 73, Cordemex, Mérida Yuc., México

Received December 14, 1995; in revised form March 20, 1996; accepted April 1, 1996

The double oxides of the lanthanides and tantalum $LnTa_3O_9$ (Ln = Tb, Eu) were synthesized by solid state reaction and characterized by X-ray powder diffraction. $EuTa_3O_9$ is orthorhombic, with space group *Pmmm*, $a = 3.8689(3)$ Å, $b = 3.8837(2)$ Å, $c = 7.7972(1)$ Å, $V = 117.158$ Å^3, $Z = 2/3$; $TbTa_3O_9$ is tetragonal, with space group *P4/mmm*, $a = 3.8603(2)$ Å, $c = 7.7804(3)$ Å, $V = 115.943$ Å^3, $Z = 2/3$. The continuous solid solution $Tb_{1-x}Eu_xTa_3O_9$ were obtained and characterized. Cell parameters and density measurements of 10 specimens of solid solutions as a function of x are presented.

INTRODUCTION

Perovskite structure double oxides have been studied by a number of workers because of their interesting optical and electrical properties. In the perovskite structure, the double oxides containing lanthanides and niobium or tantalum ions, with the formula $LnNb(Ta)O_3$ have the Ln sites completely filled, and they present interesting dielectric behavior (1, 2). In the case for double oxides $LnTa_3O_9$ reported here, the lattice has Ln vacant sites. From the crystallochemical point of view, it is interesting to provide information on the influence of defects on the stability of the crystal lattice and more specifically, it is important to look for the relationship between crystal structure and dielectric properties in those related perovskite structures.

On the other hand, for spectroscopic studies, nonradiative energy transfer processes involving trivalent lanthanide ions in inorganic solids have been widely studied in recent years, but the majority of the investigations have dealt with the Ln^{3+} ions at low symmetry sites (3).

Electrical and optical properties of similar compounds ($LnNb_3O_9$; Ln = La, Ce, Pr, and Nd) have also been reported (4–7).

Among the several possibilities in this perovskite family, in this work the rare earth tantalates $TbTa_3O_9$ and their continuous solid solution $Tb_{1-x}Eu_xTa_3O_9$ were synthesized and characterized, because of the interesting features of the energy transfer processes between Tb^{3+} and Eu^{3+} (8).

EXPERIMENTAL

The starting materials were terbium (III) carbonate hydrate (99.9%, Aldrich), tantalum (V) oxide (99.99%, Aldrich), and europium (III) oxide (99.999%, Aldrich). Compounds were prepared by solid state reaction, with initial firing at 700°C for a few hours to expel CO_2. All the samples were finally fired at 1500°C for a period of 20 to 25 days. The products of reaction were identified by X-ray powder diffraction using a Siemens D5000 diffractometer ($CuK\alpha_1$ radiation, $\lambda = 1.54060$ Å), and a secondary graphite monochromator. Density measurements were made with specific gravity bottles using CCl_4 as displacement liquid.

The lattice parameters of the samples were determined with measurements in the range of $5 \leq 2\theta \leq 100$ degrees with a step width of 0.02° for 2θ; counting time per step was 1 s. For refinement studies the reflections were measured in

0022-4596/96 $18.00

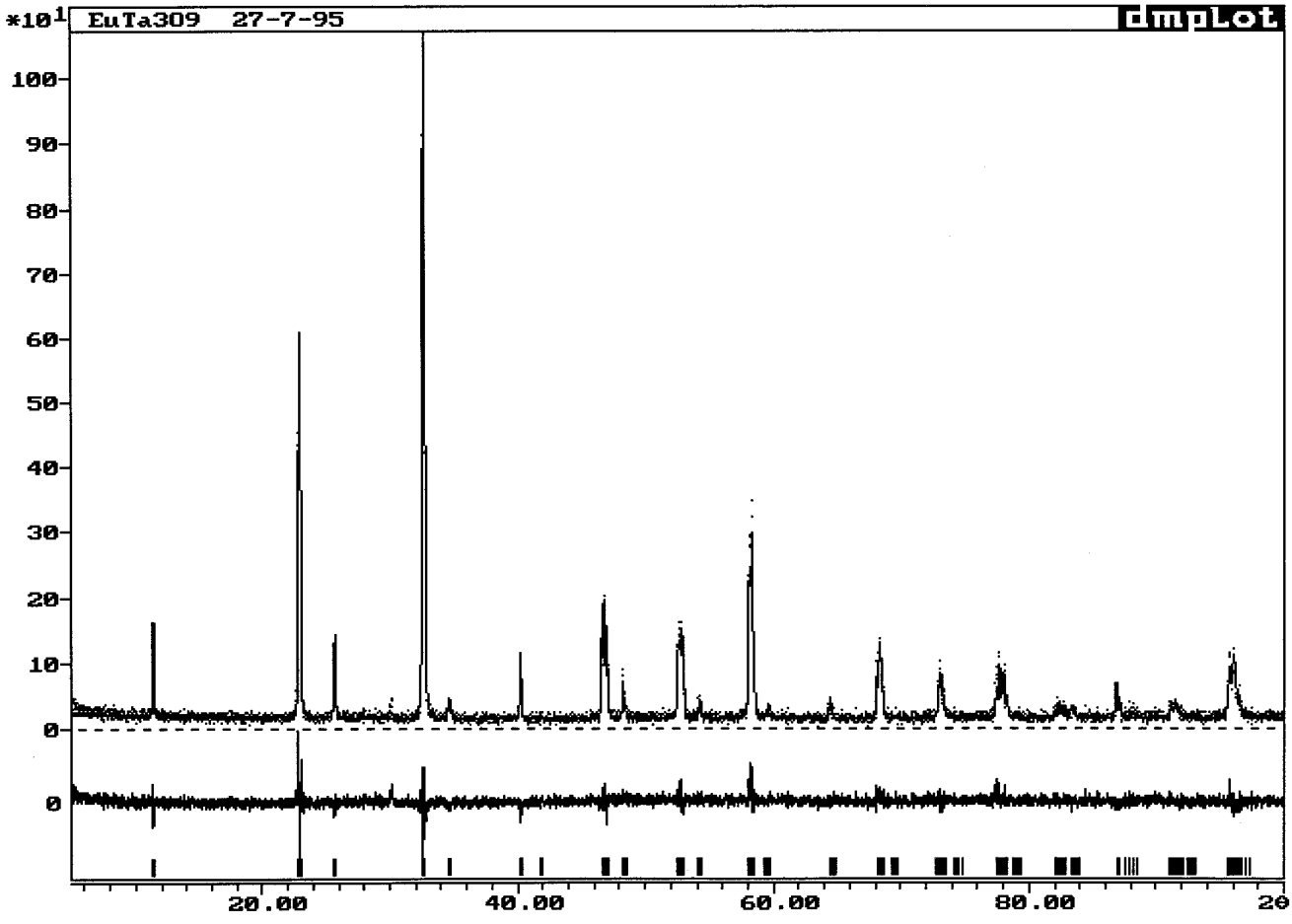

FIG. 1. X-ray refined powder diffraction pattern of $EuTa_3O_9$.

the same conditions but counting time per step was 10 s. The data were corrected using Si as an external standard with $a = 5.4306(4)$ Å at 25°C and subtracted $k\alpha_2$ before reading 2θ and the intensities.

The computer program DIFFRACT/AT (11) was applied to obtain well resolved powder lines. The TREOR program (12) was used for indexing and LSUCRI (13) was used for cell refinements. The refinement using the Rietveld method was carried out using the DBWS-9006PC program (14). The employed profile was a pseudo-Voigt function. The final R_w was 0.12 (12%) for both compounds. The determination of the crystal structure from powder data was based on the isostructural compound $LaTa_3O_9$ (15).

DISCUSSION

The experimental data for the interplanar spacing, the relative intensities, and the (*hkl*) indices of the $EuTa_3O_9$ and the $TbTa_3O_9$ compounds are shown in Tables 1 and 2. The powder diffraction patterns with the observed and the calculated intensities and the difference between them are shown in Figs. 1 and 2. The compounds have a perovskite related structure with the lanthanides (Eu and Tb) in dodecahedral sites and the Ta^{5+} ions in octahedral sites.

The crystal data are shown in Table 3. Tables 4A, 4B, 5A, and 5B show the refinement data including the crystallographic positions and the thermal parameters of the Rietveld analysis for both compounds.

Figure 3 is a schematic projection of the $EuTa_3O_9$ structure obtained using the Cerius[2] program (16).

The continuous solid solution has a structural change: it is orthorhombic for $x \geq 0.5$ and tetragonal for $x < 0.5$. The variation in the lattice parameters of the parent compounds $EuTa_3O_9$ and $TbTa_3O_9$ and the data of 10 specimens of the solid solution, as function of x, are shown in Tables 6A and 6B and in Fig. 4 (17).

Densities (ρ) of 10 specimens of the solid solution were measured. These results are shown in Fig. 5. In the same figure, the calculated values of ρ using the solid solution

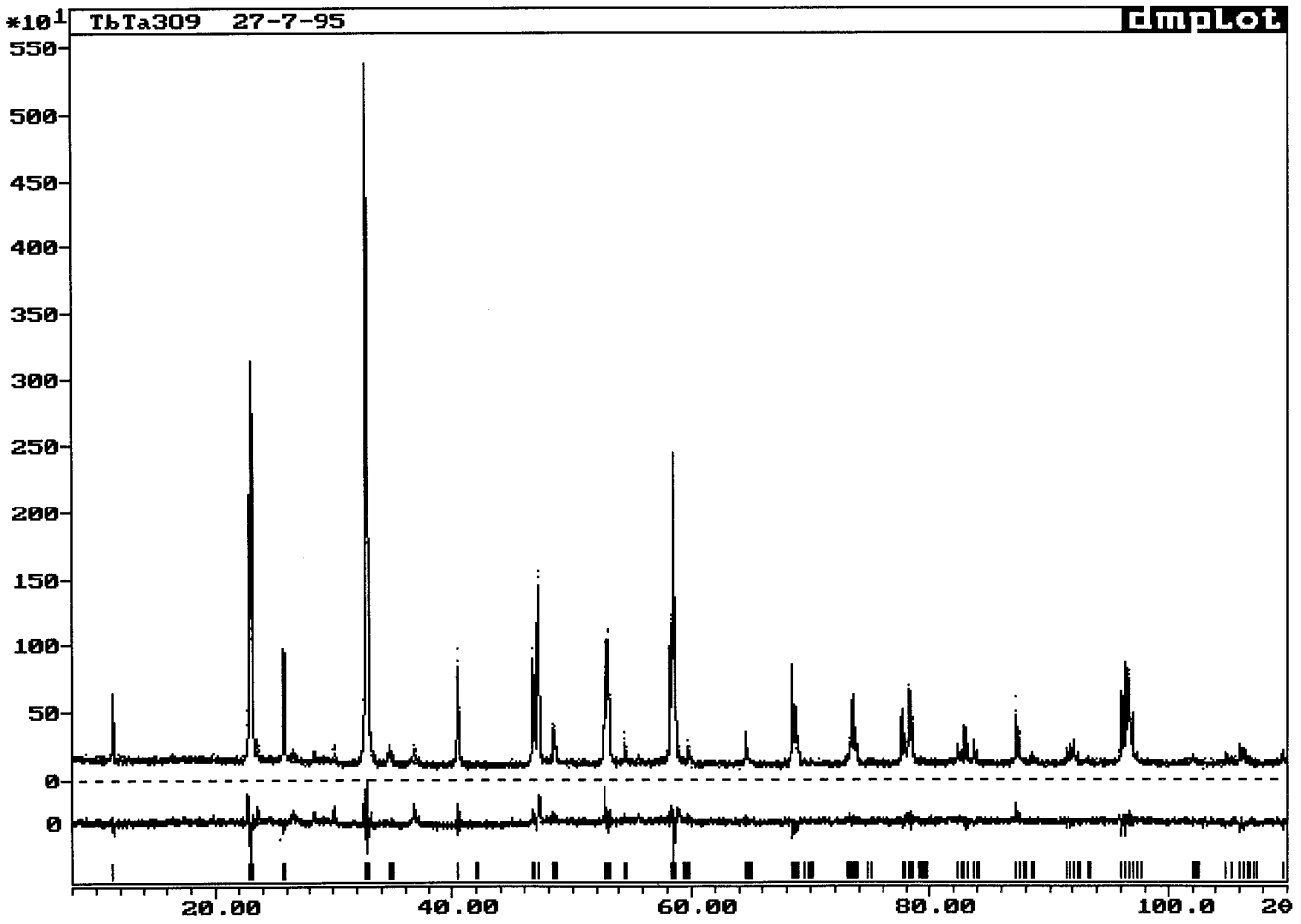

FIG. 2. X-ray refined powder diffraction pattern of $TbTa_3O_9$.

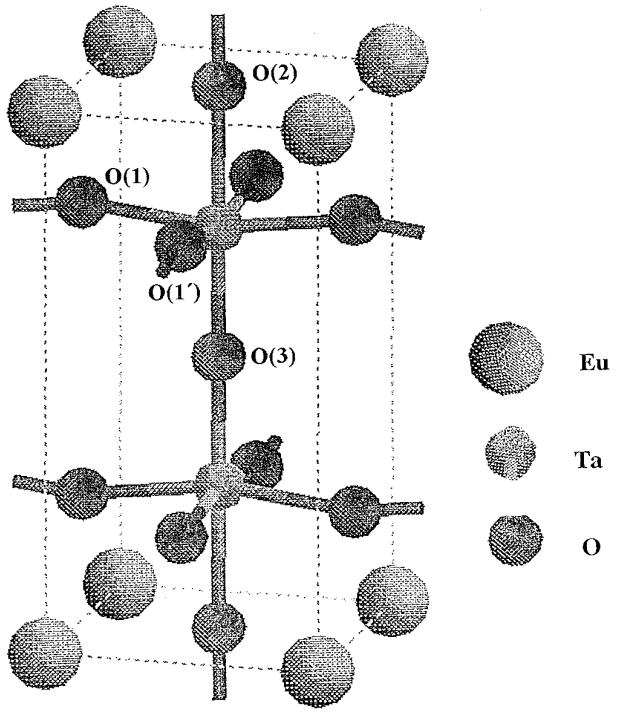

FIG. 3. The unit cell of $EuTa_3O_9$.

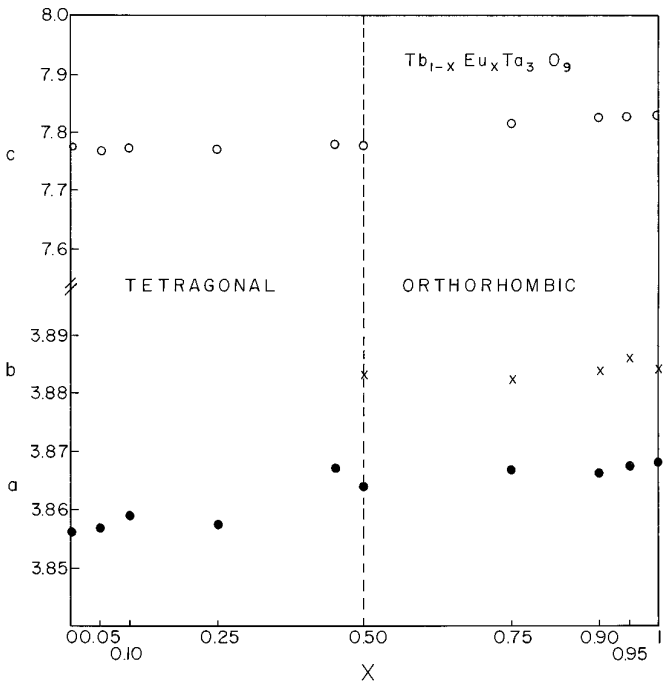

FIG. 4. The cell parameters for the $Tb_{1-x}Eu_xTa_3O_9$ solid solution.

TABLE 1
X-Ray Data for $EuTa_3O_9$

$2\theta(°)$	d(Å)	I/I_o	hkl
11.360	7.7829(8)	10	001
22.878	3.8840(4)	49	010
25.699	3.4637(2)	11	101
32.615	2.7433(1)	50	102
32.647	2.7406(9)	100	110
34.672	2.5851(2)	3	111
40.214	2.2407(1)	10	112
46.739	1.9419(7)	16	020
46.944	1.9339(6)	14	200
48.261	1.8842(2)	9	021
48.265	1.8840(7)	7	113
52.699	1.7355(1)	15	120
54.236	1.6899(1)	4	211
58.286	1.5817(5)	26	212
59.577	1.5505(2)	3	203
64.435	1.4448(5)	4	015
64.477	1.4440(1)	4	105
68.170	1.3745(0)	10	024
68.405	1.3703(5)	12	220
73.108	1.2933(6)	7	214
73.162	1.2925(4)	9	222
77.524	1.2303(4)	10	016
77.563	1.2298(2)	7	106
77.666	1.2284(5)	9	032
77.722	1.2277(0)	8	130
78.010	1.2238(9)	9	302
78.028	1.2236(5)	8	310
82.143	1.1724(5)	3	116
82.282	1.1708(2)	3	132
83.327	1.1587(7)	3	125
83.358	1.1584(2)	3	033
86.872	1.1203(7)	7	224
95.786	1.0382(9)	13	134
96.087	1.0358(3)	9	314

mechanism $Tb^{3+} \leftrightarrow Eu^{3+}$, giving a solid solution formula $Tb_{1-x}Eu_xTa_3O_9$, in which the total number of cations is constrained to remain constant, is also included for the sake of comparison. The experimental density values are generally 1 to 3% smaller than the theoretical values calculated for the proposed replacement mechanisms. This effect is common for measurements of the densities of powders using liquid displacement and it is attributed to the difficulty in removing residual air trapped on the surface of the particles. However, the important result is that the experimental data run approximately parallel to the theoretical line, indicating the correctness of the proposed solid solution mechanism.

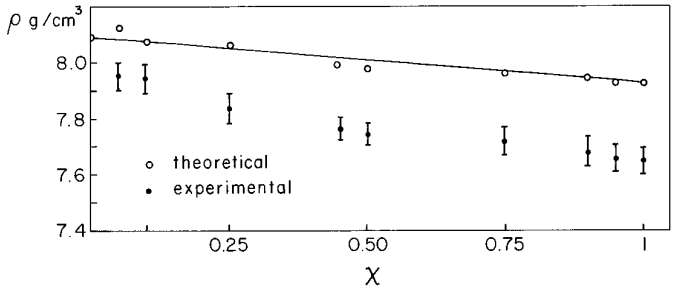

FIG. 5. Density data for the $Tb_{1-x}Eu_xTa_3O_9$ solid solution.

TABLE 2
X-Ray Data for $TbTa_3O_9$

$2\theta(°)$	d(Å)	I/I_o	hkl
11.337	7.7985(8)	11	001
22.854	3.8880(6)	29	002
23.056	3.8544(5)	60	010
25.770	3.4536(7)	19	101
32.692	2.7370(2)	100	012
32.860	2.7234(1)	54	110
34.599	2.5904(1)	4	003
34.833	2.5735(4)	3	111
40.387	2.2315(1)	14	112
46.693	1.9437(8)	17	004
47.109	1.9275(8)	32	020
48.423	1.8782(9)	9	113
48.657	1.8698(1)	4	021
52.691	1.7357(6)	14	014
52.979	1.7270(0)	19	022
53.075	1.7241(0)	7	120
54.468	1.6832(5)	6	121
58.256	1.5825(0)	25	114
58.514	1.5761(3)	48	122
59.734	1.5468(2)	3	023
64.553	1.4424(9)	5	015
68.487	1.3689(1)	17	024
68.821	1.3630(8)	9	220
69.729	1.3475(3)	2	115
70.019	1.3426(6)	3	221
72.929	1.2960(9)	3	006
73.329	1.2900(1)	12	124
73.569	1.2863(9)	8	222
73.649	1.2851(9)	4	030
74.817	1.2680(0)	6	031
77.658	1.2285(5)	12	016
78.362	1.2192(7)	12	130
78.284	1.2202(9)	6	032
79.352	1.2065(2)	3	223
79.508	1.2045(5)	2	131
82.302	1.1705(9)	4	116
82.922	1.1634(0)	6	132
83.672	1.1548(7)	5	125
87.278	1.1161(9)	11	224
87.791	1.1109(9)	6	007
88.558	1.1033(4)	3	133
91.470	1.0756(6)	3	026
91.853	1.0721(7)	4	034
92.160	1.0694(2)	4	230

TABLE 3

	$EuTA_3O_9$	$TbTa_3O_9$
	Symmetry classifications	
Crystallographic system	Orthorhombic	Tetragonal
Space group	*Pmmm*	*P*4/*mmm*
Pattern symmetry	*mmm*	4/*mmm*
	Data collection and analysis parameters	
Radiation	Cu$K\alpha$	Cu$K\alpha$
Filter	Graphite monochromator	Graphite monochromator
Angle	$2\theta = 8° - 110°$	$2\theta = 8° - 110°$
Wavelength	1.5406 Å	1.5406 Å
Approx. temp.	296 K	296 K
	Crystallographic constants	
a	3.8689(3) Å	3.8603(2) Å
b	3.8837(2) Å	
c	7.7972(1) Å	7.7804(3) Å
V	117.158 Å^3	115.943 Å^3
Z	2/3	2/3
F.W.	838.7983 g/mol	845.7637 g/mol
D_x	7.92 g/cm^3	8.07 g/cm^3
D_m	7.63 g/cm^3	8.10 g/cm^3
	Structure refinement *R*-factors	
R	0.092 (9.16%)	0.098 (9%)
R_w	0.117 (11.7%)	0.12 (12%)
R_{exp}	8.09	8.09
S	1.45	1.58
	Bond lengths (Å)	
Tb–O	2.645(2)	2.679(2)
Ta–O	1.950(2)	1.938(3)
	2.040(2)	2.031(2)
	1.859(4)	1.859(2)
O–O	2.741(3)	2.730(3)
	Bond angle	
O–Ta–O	165.7°	169.7°

TABLE 4A
Positional Parameters for $EuTa_3O_9$ in *Pmmm*

	x/*a*	*y*/*b*	*z*/*c*	*B*(Å^2)
2/3 Eu in (a)	0	0	0	2.596(2)
2 Ta in (t)	0.5	0.5	0.2615(2)	1.441(3)
2 O(1) in (s)	0.5	0	0.2306(2)	0.767(4)
2 O(1′) in (r)	0	0.5	0.2306(2)	0.767(4)
1 O(2) in (f)	0.5	0.5	0	2.529(3)
1 O(3) in (h)	0.5	0.5	0.5	5.250(3)

Note. Standard deviation in parentheses.

TABLE 4B
Thermal Parameters for $EuTa_3O_9$

	b_{11}	b_{22}	b_{33}
Eu	−0.01042	0.00128	0.00171
Ta	0.1325	0.01481	0.00364
O(1)	−0.05272	0.11411	0.00818
O(1′)	−0.05272	0.11411	0.00818
O(2)	−0.02746	0.01113	−0.01451
O(3)	−0.05939	0.04258	−0.02490

TABLE 5A
Positional Parameters for $TbTa_3O_9$ in *P4/mmm*

	x/*a*	*y*/*b*	*z*/*c*	*B*(Å^2)
2/3 Tb in (a)	0	0	0	2.105(2)
2 Ta in (h)	0.5	0.5	0.2610(2)	0.9724(3)
4 O(1) in (i)	0	0.5	0.2387(2)	0.6728(2)
1 O(2) in (c)	0.5	0.5	0	0.7293(2)
1 O(3) in (d)	0.5	0.5	0.5	0.5141(3)

Note. Standard deviation in parentheses.

TABLE 5B
Thermal Parameters for $EuTa_3O_9$

	b_{11}	b_{22}	b_{33}
Tb	0.00001	0.00307	0.00012
Ta	0.18500	0.13840	0.00261
O(1)	−0.08131	0.16729	0.02557
O(2)	0.07740	0.98099	−0.31457
O(3)	0.93330	0.00361	−0.08007

TABLE 6A
Cell Parameters and Densities of the Orthorhombic Phases in the Solid Solution $Tb_{1-x}Eu_xTa_3O_9$

x value	*a*(Å)	*b*(Å)	*c*(Å)	*V*(Å^3)	d_{exp} (g/cm^3)	d_{calc} (g/cm^3)
1.00	3.8679(1)	3.8839(1)	7.7828(3)	116.92(1)	7.63	7.94
0.95	3.8677(6)	3.8858(5)	7.783(1)	116.99(2)	7.66	7.94
0.90	3.8661(7)	3.8835(8)	7.783(1)	116.87(2)	7.69	7.95
0.75	3.8668(5)	3.8824(5)	7.782(1)	116.84(2)	7.69	7.96
0.50	3.864(1)	3.883(2)	7.778(2)	116.75(6)	7.75	7.98

TABLE 6B
Cell Parameters and Densities of the Tetragonal Phases in the Solid Solution $Tb_{1-x}Eu_xTa_3O_9$

x value	*a* = *b* (Å)	*c* (Å)	*V* (Å^3)	d_{exp} (g/cm^3)	d_{calc} (g/cm^3)
0.45	3.8681(5)	7.789(1)	116.54	7.76	8.00
0.25	3.8575(5)	7.774(1)	115.69(3)	7.84	8.07
0.10	3.8588(4)	7.774(1)	115.77(2)	7.94	8.08
0.05	3.8571(7)	7.773(1)	115.12(3)	7.95	8.13
0.00	3.8555(1)	7.7765(3)	115.598(7)	8.10	8.10

ACKNOWLEDGMENTS

We thank DGIA (UNAM) and CONACyT for travel assistance through the México–Cuba collaboration programme, and DGAPA, UNAM for support through the PAPIIT program. We also thank R. Reyes and S. Jimenez for technical assistance.

REFERENCES

1. F. Iona and D. Shirane, ''Segnetoelectric Crystals.'' Mir, Moscow, 1965.
2. N. N. Krainik, H. Bielska-Lewandowska, and I. E. Mylnikova, *Chan-Van-Tiau, A* **38**(6), 849 (1970).
3. J. Rubio O., *Revista Mexicana de Física,* **35**(4), 552 (1989).
4. E. Orgaz and A. Huanosta, *J. Solid State Chem.* **97,** 65 (1992).
5. A. Huanosta and E. Orgaz, *Solid State Ionics.* **62,** 69 (1993).
6. H. G. C. Verhaar, H. Donker, G. Dirksen, M. J. J. Lammers, G. Blasse, C. C. Torardi, and L. H. Brixner, *J. Solid State Chem.* **60,** 20 (1985).
7. C. C. Torardi, L. H. Brixner, and C. M. Foris, *J. Solid State Chem.* **58,** 204 (1985).
8. M. Bettinelli and C. D. Flint, *J. Condens. Matter,* **2,** 8417 (1990).
9. V. P. Sirotinkin, A. A. Evdokimov, and Kh. G. Tadzhi-Aglaev, *Russ. J. Inorg. Chem.* **29**(6), 829 (1984).
10. H. P. Rooksby, E. A. D. White, and S. A. Langston, *J. Am. Ceram. Soc.* **48**(9), 447 (1965).
11. DIFFRAC/AT/V3.2 Copyright (c) SOCABIM 1986, 1993-Copyright (c) SIEMENS (1993).
12. P. E. Werner, L. Eriksson, and M. Westdahl, *J. Appl. Crystallogr.* **18,** 367 (1985).
13. R. G. Garvey, LSUCRI, *Powder Diff.* **1,** 114 (1986).
14. A. Sakthivel and R. A. Young, ''DBWS-9006PC/Program for Rietveld Analysis of X-Ray and Neutron Powder Diffraction Patterns.'' School of Physics, Georgia Institute of Technology, 1992.
15. P. N. Iyer and A. J. Smith, *Acta Crystallogr.* **23,** 740 (1967).
16. The results were generated using the program Cerius^2. This program was developed by Molecular Simulations Incorporated, U.S.A.
17. M. E. Villafuerte-Castrejón, A. Ibarra-Palos, M. A. Leyva, J. Duque, and R. Pomés, *in* ''Proceedings of the Fourth Euro Ceramics, Electroceramics'' (G. Gusmano and E. Traversa, Eds.), Vol. 5, pp. 81–88. Faenza, Italy, 1995.